Dynamics of two-photon paired superradiance

M. Yoshimura,[1,*] N. Sasao,[2,†] and M. Tanaka[3,‡]

[1]*Center of Quantum Universe, Faculty of Science, Okayama University, Tsushima-naka 3-1-1 Kita-ku, Okayama 700-8530, Japan*

[2]*Research Core for Extreme Quantum World, Okayama University, Tsushima-naka 3-1-1 Kita-ku, Okayama 700-8530, Japan*

[3]*Department of Physics, Graduate School of Science, Osaka University, Toyonaka, Osaka 560-0043, Japan*

(Received 2 April 2012; published 9 July 2012)

We develop for dipole-forbidden transition a dynamical theory of two-photon paired superradiance (PSR). This is a cooperative process characterized by two photons emitted back to back with equal energies. By irradiating the trigger laser from two target ends, with its frequency tuned at the half energy between two levels, a macroscopically coherent state of medium and fields dynamically emerges as time evolves, and a large signal of amplified output occurs with a time delay. The basic semiclassical equations in $1+1$ space-time dimensions are derived for the field-plus-medium system to describe the space-time evolution of the entire system and are numerically solved to demonstrate the existence of both explosive and weak PSR phenomena in the presence of relaxation terms. The explosive PSR event terminates accompanying a sudden release of most of the energy stored in the target. Our numerical simulations are performed using the vibrational transition $X^1\Sigma_g^+ v=1\rightarrow 0$ of a para-H_2 molecule and taking many different excited atom number densities and different initial coherences between the metastable and the ground states. In an example with a number density close to $O(10^{21}\ \mathrm{cm}^{-3})$ and a high initial coherence, the explosive event terminates several nanoseconds after the trigger irradiation, when the phase relaxation time larger than $O(10\ \mathrm{ns})$ is taken. After PSR events the system is expected to follow a steady-state solution which is obtained by analytic means and is made of many objects of field condensates endowed with a topological stability.

DOI: 10.1103/PhysRevA.86.013812 PACS number(s): 42.50.Nn, 42.50.Gy, 42.65.Sf

I. INTRODUCTION

Since their early suggestion [1] a variety of coherent two-photon processes have attracted much interest, from both the theoretical [2–4] and experimental sides [5–9]. Our present work is focused on a different aspect of coherent two-photon emission from Λ-type three-level atoms (or molecules) where the transition between two lower levels is dipole forbidden (see Fig. 1 for the level structure). As pointed out in Ref. [10], a macroscopic target made of metastable atoms in $|e\rangle$ in Fig. 1 may induce a characteristic event of macrocoherent two-photon emission, two photons emitted exactly back to back with equal energies. We use for this phenomenon the terminology of two-photon paired superradiance (PSR). The term paired is used because two emitted photons are highly correlated in their momenta and spin orientations (most clearly seen in the $J=0\rightarrow 0$ transition). The rate enhancement factor in the momentum configuration of the back-to-back emission is expected to be much larger than in the usual superradiance (SR) case [11] due to the lack of a wavelength limitation there: the coherent volume for SR is limited with the wavelength λ by $\lambda^2 L$, where L is the target length for a cylindrical configuration, while the macrocoherent PSR has the coherent volume of the entire cylinder irradiated by the trigger.

The usual single-photon superradiance occurs irrespective of the absence or presence of a trigger due to the intrinsic instability of exponential spontaneous decay caused by dipole-allowed transition. On the other hand, two-photon emission occurs with a much smaller rate in the higher order of perturbation beyond the dipole-forbidden transition; hence the use of a trigger is essential to assist the macrocoherence development for the two-photon process and to induce rapid PSR events with a large signal. Quantum initiation such as that proposed for SR in Ref. [12] is not needed since PSR is more akin to the triggered SR [13], which makes the following semiclassical treatment appropriate.

A basic formalism of two-photon process already exists for propagation equations [3] and for analytic results [14] of the propagation problem and PSR emission treated as perturbation. But this formulation turns out to be insufficient to dynamically discuss (back to back) two-mode propagation incorporating PSR, which seems essential for a dense medium. In the present work we shall be able to derive a fundamental set of semiclassical equations for the two modes and further present formulation of a two-color problem. The essential ingredient in our work is the derivation of a more general quantum-mechanical equation for both the medium (Bloch equation) and the electromagnetic field (extension of the quantum Maxwell equation to include the two-photon process). After elucidating the nature of the quantum state of fields and the medium, namely, a time-evolving electric-field condensate, we shall go on to the semiclassical equation. In this way we determine how back-to-back two modes are precisely coupled beyond the perturbation theory.

We ignore the granularity and rely on the continuum limit formulation of the atom distribution, taking one spatial dimension alone, because the whole event is highly focused on one direction of the irradiated trigger field taken as the x direction. The system of semiclassical partial differential equations thus derived is highly nonlinear and must generally be analyzed with numerical simulations. In this way we find explosive and weak PSR phenomena and under what conditions these may occur.

Despite its complicated nonlinearity the system allows soliton solutions of two kinds, which are obtained as

*yoshim@fphy.hep.okayama-u.ac.jp
†sasao@fphy.hep.okayama-u.ac.jp
‡tanaka@phys.sci.osaka-u.ac.jp

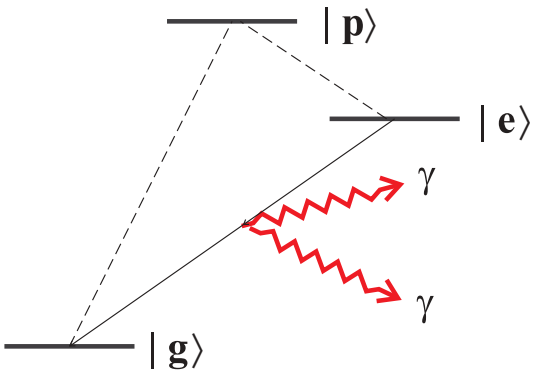

FIG. 1. (Color online) Λ-type atomic level for PSR. The dipole-forbidden transition $|e\rangle \to |g\rangle + \gamma + \gamma$ may occur via strong $E1$ couplings to $|p\rangle$.

steady-state solutions of this nonlinear system of fields and medium. Solitons here, in their field part, are an electric-field condensate which may or may not be moving: there can be a static-field condensate. The stability (against two-photon emission) of solitons is ensured by a topological quantum number, as explained in the text below. Our conjecture, which is supported by numerical simulations but not established by a more rigorous method, is that the field condensate formed after rapid PSR phenomena is made of many topological solitons. After the formation of field condensates, namely, a stable target state against two-photon emission, the light may propagate almost freely. The condensate state of the field plus medium thus formed may be very useful to detect a much weaker process, such as radiative neutrino pair emission (RNPE) [15], because the condensate is not stable against RNPE.

A related propagation and soliton formation problem in the single-photon case is the phenomena of self-induced transparency (SIT) [16] and electromagnetically induced transparency (EIT) [8], presumably related to solitons of the kind in Ref. [17], both at a resonant frequency. Both of these transparency phenomena thus appear to be directly related to the formation of stable solitons of different kinds than ours.

For the numerical computations below, we use parameters relevant to a good target candidate for PSR detection, the para-H_2 molecule. We have in mind using the para-H_2 vibrational transition of $X^1\Sigma_g^+ v = 1 \to 0$ (X being the electronic ground molecular state). Many other atoms and molecules are conceivable for PSR experiments. The characteristic length scale for large effects is ∼14 cm, and the time scale is ∼0.5 ns for para-H_2 with a molecule density of $n = 10^{20}$ cm^{-3}. The number density dependence of these characteristic parameters is $\propto 1/n$. We include relaxation effects of two time constants in the range of $T_2 \geqslant 10$ ns (a feasible value experimentally) and $T_1 \gg T_2$ in our analysis. The origin of these relaxation constants is left unexplained, and in this way one may use values experimentally measured by other means. We perform extensive numerical simulations in order to clarify experimentally observable PSR signals and condensate formation in forthcoming experiments. It is demonstrated that an explosive PSR emission occurs for long targets even for a weak trigger when initial coherence between states, $|e\rangle$ and $|g\rangle$, is present. We have identified two different types of PSR events caused by trigger irradiation: (1) explosive PSR, in which most of the stored energy in the initial metastable state $|e\rangle$ is released as a short pulse of some time structure, and (2) weak PSR, in which the output energy flux is in linear proportion to the trigger power. The natural unit $\hbar = c = 1$ is used throughout the present paper.

II. DERIVATION OF QUANTUM AND SEMICLASSICAL EQUATIONS

Consider a three-level atom (or molecule) of energies $\epsilon_p > \epsilon_e > \epsilon_g$, as shown in Fig. 1. We assume that the transition between two lower levels, $|e\rangle$ and $|g\rangle$, is dipole forbidden. Suppose that the upper level $|p\rangle$ has substantial $E1$ rates for both $|e\rangle$ and $|g\rangle$. (This can be replaced by a weaker $M1$ transition since the relation we need subsequently is the partial decay rate $\propto \epsilon_{ij}^3$ with the energy level difference $\epsilon_{ij} = \epsilon_i - \epsilon_j$, which holds in both the $E1$ and $M1$ cases.)

We focus on, and derive an effective Hamiltonian of, the two lower levels interacting with the oscillating electric field E. Its Hamiltonian density has been derived in Refs. [3,14] for a single mode of field, such as a light wave of definite frequency traveling in one direction. The extension to multimode fields, such as counterpropagating modes of the same frequency, is given in Appendix A. Its Hamiltonian has the form of a 2×2 matrix acting on two atomic states, $|e\rangle$ and $|g\rangle$, $\sim E\mathcal{M}E$. The multimode field E may be decomposed into positive- and negative-frequency parts, $E = \sum_j \frac{1}{2}(E_j^* e^{i\omega_j t} + E_j e^{-i\omega_j t})$, where E_j, E_j^* are slowly varying envelopes in time. We shall use the variables $E_j^+ = E_j e^{-i\omega_j t}$ and $E_j^- = E_j^* e^{i\omega_j t}$ to simplify the formulas given below. In quantum field theory E_j and E_j^* represent annihilation and creation operators of the definite mode. The pertinent Hamiltonian to our discussion of the single mode is

$$\frac{d}{dt}\begin{pmatrix} c_e(x,t) \\ c_g(x,t) \end{pmatrix} = -i\mathcal{H}_I \begin{pmatrix} c_e(x,t) \\ c_g(x,t) \end{pmatrix}, \tag{1}$$

$$-\mathcal{H}_I = \begin{pmatrix} \mu_{ee} E^+ E^- & e^{i\epsilon_{eg}t}\mu_{ge}(E^+)^2 \\ e^{-i\epsilon_{eg}t}\mu_{ge}(E^-)^2 & \mu_{gg} E^+ E^- \end{pmatrix}, \tag{2}$$

$$\mu_{ge} = \frac{2d_{pe}d_{pg}}{\epsilon_{pg} + \epsilon_{pe}}, \quad \mu_{aa} = \frac{2d_{pa}^2 \epsilon_{pa}}{\epsilon_{pa}^2 - \omega_0^2} \quad (a = g,e), \tag{3}$$

where $|c_e|^2 + |c_g|^2 = n(x)$, with $n(x)$ being the number density of atoms per a unit volume in a linear target region of $0 \leqslant x \leqslant L$. For simplicity we took an isotropic medium and linearly polarized fields, taking $\vec{E}^{\pm}$ as scalar functions. The diagonal part $\propto \mu_{aa}$ of this Hamiltonian describes ac Stark energy shifts, while the off-diagonal parts $\propto \mu_{ge}$ are for two-photon emission and absorption.

For a p-H_2 target the photon energy $\omega_0 = \epsilon_{eg}/2$ (∼0.26 eV) is much smaller than level spacings of the electronically excited intermediate states; both ϵ_{pe} and ϵ_{pg} are ∼11 eV. Under this condition we may ignore ω_0 compared to $\epsilon_{pa}, a = e,g$ in the formula for μ_{ab} and identify μ_{ab} with the polarizability for which a precision calculation exists [18]. We thus use numerical values of parameters, $\mu_{gg} \sim 0.80, \mu_{ee} \sim 0.87$, and $\mu_{ge} \sim 0.055$, all in units of 10^{-24} cm^3 [19], for the p-H_2 $Xv = 1 \to Xv = 0$ transition.

The density matrix of pure atomic states, $\rho = |\psi(x,t)\rangle\langle\psi(x,t)|$ $[\langle\psi(x,t)| = (c_e, c_g)]$, obeys the evolution

equation $\partial_t \rho = -i[\mathcal{H}_I, \rho]$. This quantum-mechanical equation is generalized to include dissipation or relaxation. The needed variable, the density matrix for the mixed state, is given by a statistical mixture of pure states:

$$\rho(x,t) = \sum_i c_i |\psi_i(x,t)\rangle\langle\psi_i(x,t)|, \qquad \sum_i c_i = 1, \quad 0 \leqslant c_i \leqslant 1, \tag{4}$$

with $|\psi_i(x,t)\rangle$ being a set of orthonormal pure-state vectors. Dissipation occurs when a subsystem of $|e\rangle, |g\rangle$ interacts with a reservoir, and we integrate out reservoir variables due to our basic ignorance of the reservoir. The general form of mixed-state evolution including dissipation has been derived by Lindblad [20], assuming the general principle of positivity and conservation of probability. As a result the time-evolution equation of the density matrix has an additional operator term, $L[\rho]$. The new additional dissipation term in the two-level atomic system turns out to be equivalent to phenomenological relaxation terms given by two time constants, T_1 and T_2 (with the constraint $T_1 > T_2/2$ from consistency with [20]).

It is convenient to write the evolution equations in terms of components of the Bloch vector defined by $\vec{R} = \mathrm{tr}\,\rho\vec{\sigma} = \langle\psi|\vec{\sigma}|\psi\rangle$. The basic Bloch equation including relaxation terms is

$$\partial_t R_1 = (\mu_{ee} - \mu_{gg})E^+E^-R_2 - i\mu_{ge}(e^{i\epsilon_{eg}t}E^+E^+ - e^{-i\epsilon_{eg}t}E^-E^-)R_3 - \frac{R_1}{T_2}, \tag{5}$$

$$\partial_t R_2 = -(\mu_{ee} - \mu_{gg})E^+E^-R_1 + \mu_{ge}(e^{i\epsilon_{eg}t}E^+E^+ + e^{-i\epsilon_{eg}t}E^-E^-)R_3 - \frac{R_2}{T_2}, \tag{6}$$

$$\partial_t R_3 = \mu_{ge}[i(e^{i\epsilon_{eg}t}E^+E^+ - e^{-i\epsilon_{eg}t}E^-E^-)R_1 - (e^{i\epsilon_{eg}t}E^+E^+ + e^{-i\epsilon_{eg}t}E^-E^-)R_2] - \frac{R_3 + n}{T_1}. \tag{7}$$

$T_1 \gg T_2$ usually, and the phase decoherence time T_2 is much smaller and more important than the decay time T_1, which may be taken to be infinitely large for our practical purpose.

Derivation of the quantum field equation follows a similar line of reasoning. To perform the derivative operation ∂_t^2 as in the Maxwell equation, one needs to calculate the double commutator:

$$\partial_t^2 \vec{E}^{\pm} = -[H,[H,\vec{E}^{\pm}]], \quad H = \int d^3x(\mathcal{H}_f + \mathrm{tr}\,\rho\mathcal{H}_I), \tag{8}$$

with the field energy density $\mathcal{H}_f = (\vec{E}^2 + \vec{B}^2)/2$. For convenience we add less dominant oscillating terms of the field modes to $E^{\pm}$ and use the locally well-behaved field $E(x,t)$ in $\mathcal{H}_I$. The fundamental commutation relation in the radiation gauge QED $[E_y(\vec{r},t), B_z(\vec{r}',t)] = i\partial_x\delta^3(\vec{r} - \vec{r}')$ [21] is used to derive the quantum field equation. The result is

$$\left(\partial_t^2 - \vec{\nabla}^2\right)\vec{E}^{\pm} = \vec{\nabla}^2\mathcal{D}\vec{E}^{\pm}, \tag{9}$$

$$-\mathcal{D}\vec{E}^{+} = \left(\frac{\mu_{ee} + \mu_{gg}}{2}n + \frac{\mu_{ee} - \mu_{gg}}{2}R_3\right)\vec{E}^{+} + \mu_{ge}e^{-i\epsilon_{eg}t}(R_1 - iR_2)\vec{E}^{-}. \tag{10}$$

This equation [22] along with the Bloch equations (5)–(7) is the basis of the following derivation of our master equation.

A. Slowly varying envelope approximation (SVEA)

Fast oscillating terms do not contribute to global features of time and spatial evolution when one averages over a few times of spatial and time oscillation periods. We thus extract terms that persist over time periods of typical light oscillation of order $1/\omega$ both in time and space. Envelope functions denoted by E_R, E_L are amplitudes of right(R)- and left(L)-moving components of rapidly oscillating parts $\propto e^{-i\omega(t\mp x)}$.

The result of SVEA may be summarized using dimensionless units of space-time coordinates ξ, τ and dimensionless fields $e_{L,R}$ given by

$$(\xi,\tau) = (\alpha_m x, \alpha_m t), \quad \alpha_m(\omega) = \frac{\epsilon_{eg}}{2}n\mu_{ge}(\omega), \qquad |e_{L,R}|^2 = \frac{|E_{L,R}|^2}{\epsilon_{eg}n}, \quad r_i = \frac{R_i}{n}. \tag{11}$$

The quantity $1/\alpha_m = 2/(\mu_{ge}\epsilon_{eg}n)$ gives a fundamental unit of target length and time scale of evolution. Since a functional relation $\alpha_m(\omega) = \alpha_m(\epsilon_{eg} - \omega)$ holds, the propagation problem of the trigger irradiation of pair frequencies, ω and $\epsilon_{eg} - \omega$, is described by the same dimensionless quantities of a common α_m. Its value at $\omega = \epsilon_{eg}/2$ is $\sim$14 cm and $\sim$0.5 ns for para-H_2 with a density of 10^{20} cm^{-3}.

The most general fundamental equations including both nontrivial propagation and PSR effects are derived in Appendix A and are given by formulas (A35)–(A42). It is useful to recall the physical meaning of coupling constants μ_{ab} in the interaction Hamiltonian in order to fully appreciate the following approximation in our numerical simulations. Consider the extended Hamiltonian including both counterpropagating modes given by Eq. (A14) in Appendix A. We first note that annihilation (a_i) and creation ($a_i^{\dagger}$) operators of photon modes are related to complex fields by $E_i^+ \sim a_i\sqrt{\omega/2V}$, $E_i^- \sim a_i^{\dagger}\sqrt{\omega/2V}$, where V is the quantization volume. The important equations are obtained after SVEA and are given in Appendix A. They are written in terms of envelope functions:

$$(\partial_t + \partial_x)E_R = \frac{i\omega}{2}\left[\left(\frac{\mu_{ee} + \mu_{gg}}{2}n + \frac{\mu_{ee} - \mu_{gg}}{2}R_3^{(0)}\right)E_R + \frac{\mu_{ee} - \mu_{gg}}{2}R_3^{(+)}E_L + \mu_{ge}[(R_1 - iR_2)^{(0)}E_L^* + (R_1 - iR_2)^{(+)}E_R^*]\right], \tag{12}$$

$$(\partial_t - \partial_x)E_L = \frac{i\omega}{2}\left[\left(\frac{\mu_{ee} + \mu_{gg}}{2}n + \frac{\mu_{ee} - \mu_{gg}}{2}R_3^{(0)}\right)E_L + \frac{\mu_{ee} - \mu_{gg}}{2}R_3^{(-)}E_R + \mu_{ge}[(R_1 - iR_2)^{(0)}E_R^* + (R_1 - iR_2)^{(-)}E_L^*]\right]. \tag{13}$$

The right-hand sides of these equations give the effects, all in the bulk medium, of forward scattering $\propto \frac{\mu_{ee}+\mu_{gg}}{2}n + \frac{\mu_{ee}-\mu_{gg}}{2}R_3^{(0)}$, backward scattering $\propto \frac{\mu_{ee}-\mu_{gg}}{2}R_3^{(\pm)}$, right-left(RL)

pair annihilation $\propto \mu_{ge}(R_1 - iR_2)^{(0)}$, and right-right(RR) and left-left(LL) pair annihilation $\propto \mu_{ge}(R_1 - iR_2)^{(\pm)}$. (The pair creation amplitudes appear in equations conjugate to those above.) Quantities $R_i^{(\pm)}e^{\pm 2ikx}$ as defined by Eq. (A31) are what are called spatial grating in the literature. The backward scattering terms and RR- and LL-pair annihilation and creation terms are important only in the presence of spatial grating of polarization. Neglecting spatial grating is thus equivalent to retaining forward scattering and RL-pair processes and ignoring all other terms. In the simple boundary condition set up below, the backward Bragg scattering is expected to be a minor effect and is also neglected in most works on SR. We refer to Ref. [23] for the backward Bragg scattering effect in usual SR and, for instance, to Ref. [24] for the backward scattering effect on SR in low-Q cavity experiments. In a more comprehensive simulation in the future we wish to quantitatively compute the effects of the backward scattering and RR- and LL-pair processes because non-negligible differences of these effects might arise in PSR, unlike the SR case.

In the rest of the present work we shall focus on PSR effects and ignore propagation effects, which are much discussed in Refs. [3,14] and are summarized in Appendix A. The explosive PSR events discussed below are expected to be insensitive to the neglected propagation effects. The resulting Maxwell-Bloch equation for the single mode is

$$\partial_\tau r_1 = 4\gamma_-(|e_R|^2 + |e_L|^2)r_2 + 8\mathrm{Im}(e_R e_L)r_3 - \frac{r_1}{\tau_2}, \quad (14)$$

$$\partial_\tau r_2 = -4\gamma_-(|e_R|^2 + |e_L|^2)r_1 + 8\mathrm{Re}(e_R e_L)r_3 - \frac{r_2}{\tau_2}, \quad (15)$$

$$\partial_\tau r_3 = -8[\mathrm{Re}(e_R e_L)r_2 + \mathrm{Im}(e_R e_L)r_1] - \frac{r_3 + 1}{\tau_1}, \quad (16)$$

$$(\partial_\tau + \partial_\xi)e_R = \frac{i}{2}(\gamma_+ + \gamma_- r_3)e_R + \frac{i}{2}(r_1 - ir_2)e_L^*, \quad (17)$$

$$(\partial_\tau - \partial_\xi)e_L = \frac{i}{2}(\gamma_+ + \gamma_- r_3)e_L + \frac{i}{2}(r_1 - ir_2)e_R^*, \quad (18)$$

$$\gamma_\pm = \frac{\mu_{ee} \pm \mu_{gg}}{2\mu_{ge}}. \quad (19)$$

Here $\tau_i = \alpha_m T_i$ are the relaxation times in dimensionless units.

The dimensionless master equation [(14)–(18)] is governed by two important parameters, the most important of which is $\tau_2 = \alpha_m T_2$ and the next most important is $\gamma_\pm$. Another experimentally important parameter is the overall length and time $1/\alpha_m \propto 1/n$, which inversely scale with the number density n. For larger number densities of excited atoms a smaller-size target and a shorter time measurement on the order of nanoseconds becomes possible.

In terms of the two-component field φ defined below the equation reads

$$(\partial_\tau + \sigma_3\partial_\xi)\varphi - \frac{i}{2}(\gamma_+ + \gamma_- r_3)\varphi - \frac{i}{2}(r_1 - ir_2)\sigma_1\varphi^* = 0, \quad (20)$$

$$\varphi = \begin{pmatrix} e_R \\ e_L \end{pmatrix}.$$

Magnitudes of R and L fluxes change via an RL mixing term, such as

$$(\partial_\tau \pm \partial_\xi)|e_{R,L}|^2 = r_1\mathrm{Im}(e_R e_L) + r_2\mathrm{Re}(e_R e_L). \quad (21)$$

An R- or L-moving pulse alone propagates freely because we ignored in this approximation nontrivial propagation effects.

B. Quantum state of fields

As usual in quantum field theory, we may interpret $\vec{E}_{R,L}$ as annihilation operators and $\vec{E}_{R,L}^{\,\dagger}$ as creation operators. The fact that the basic equation, Eqs. (17) and (18) or (20), simultaneously contains both field annihilation and creation operators implies that the quantum state satisfying the field equation is given by a Bogoliubov transformation from the usual vacuum of the zero-photon state $|0\rangle$,

$$|\Psi\rangle = \sum_{n=0}^{\infty} c_n(x,t)(E_R^\dagger E_L^\dagger)^n|0\rangle, \quad (22)$$

where $c_n(x,t)$ is to be determined by the condition: [the left hand side of Eq. (20)] $|\Psi\rangle = 0$. The quantum state $|\Psi\rangle$ is a mixture of infinitely many states of different photon numbers. We shall not pursue this line of thought any further because we exploit the semiclassical approximation under the large quantum number limit of photons (the classical limit). The semiclassical equation is given by the expectation value of the quantum equation,

$$\langle\Psi|\left((\partial_\tau + \sigma_3\partial_\xi)\varphi - \frac{i}{2}(\gamma_+ + \gamma_- r_3)\varphi - \frac{i}{2}(r_1 - ir_2)\sigma_1\varphi^*\right) \times |\Psi\rangle = 0, \quad (23)$$

where $|\Psi\rangle$ is the Bogoliubov state given by Eq. (22). The semiclassical equation turns out to be equivalent to replacing quantum field operators in the quantum equation by the corresponding c-number functions. Equations (14)–(18), regarded as the equations for c-number functions, thus constitute the master equation for the polarization of medium and field.

In our case of a field condensate, medium polarization and fields are cooperatively involved: the target medium undergoes coherence oscillation, simultaneous with field oscillation, while keeping field envelopes slowly varying and finally almost time independent in a large time limit, as shown below. The field condensate part is technically equivalent to field state made of an infinite sum of multiple-photon pair states in the so-called coherent-state representation.

III. IMPORTANCE OF INITIAL COHERENCE

It is important to clarify in detail the ideal case of numerical solutions where all quantities in Eqs. (14)–(18) are of order unity, in the range of $O(10\text{–}1/10)$. For a deeper understanding of numerical outputs and a practical check of the accuracy of the numerical results, it is useful to know the conservation laws of our nonlinear system. We list in Appendix B all the exact and approximate conservation laws that the system possesses.

We have performed numerical simulations assuming non-pulsed continuous-wave (cw) trigger laser irradiation of the same power from two target ends (called the symmetric trigger). This boundary condition is similar, but not identical, to the one for the cavity mirror. Use of cavity mirrors has both advantages and complications. Two mirrors in a cavity automatically generate counterpropagating waves, and they effectively increase the trigger power (which, however, is not

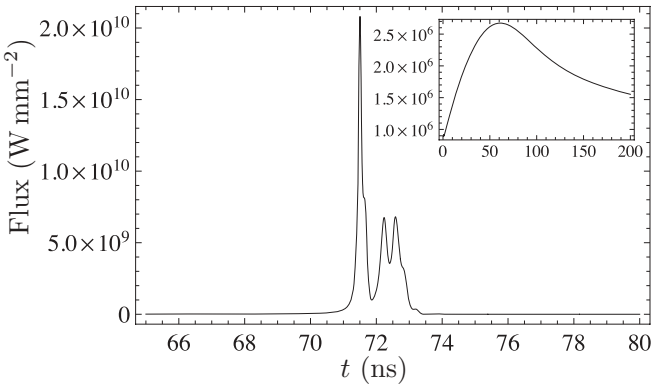

FIG. 2. Time-evolving output flux at a target end of length 30 cm resulting from the symmetric cw trigger irradiation with a power of 1 MW mm^{-2} (0.9 MW mm^{-2} in the inset). Note the large difference of $\sim 10^4$ in the output power in the two plots. Assumed parameters are $n = 1 \times 10^{21}$ cm^{-3} of p-H_2, numerical values (see the text) of μ_{ab} for the transition $Xv = 1 \rightarrow Xv = 0$, relaxation times $T_2 = 10$ ns and $T_1 = 10^3$ ns, and initial complete inversion (hence no coherence) of $r_3 = 1$ with $r_1, r_2 = 0$ taken for the initial target state.

critically needed in our case). On the other hand, each atom in the cavity is affected by the same traveling fields many times, and this complicates analysis. We use in the present work the simpler scheme of two cw counterpropagating triggers independently irradiated.

Numerical results show the symmetric output fluxes from two ends, and we exhibit in the following Figs. 2, 3, 12, and 13 one of these identical fluxes from one end. The result for the zero initial coherence $r_1(\xi,0) = r_2(\xi,0) = 0$ is shown in Fig. 2. The clear signature of a delay long after T_2 ($\sim 7T_2$ in this case) and explosive PSR is observed for strong trigger fields. It is difficult to obtain a commercially available cw laser with this power. A reason for this difficulty is that relaxation of order $T_2 \sim 10$ ns may take over the coherence development under the weak trigger usually exploited. Explosive PSR is a highly nonlinear process having a definite trigger power threshold and definitely disappears in this example at a trigger power of 0.9 MW mm^{-2}, as shown in the inset of Fig. 2.

In Fig. 2 the complete inversion to level $|e\rangle$ has been assumed as an initial condition, and it would be interesting to relax this condition and to further clarify the neglected effects of the presence of initial coherence between two atomic levels, $|e\rangle$ and $|g\rangle$. There is an experimental method to imprint an initial coherence between $|e\rangle$ and $|g\rangle$ by adopting a clever excitation scheme. The atomic state right after excitation can be made a coherent mixture of two pure states, $|e\rangle$ and $|g\rangle$, namely, $c_e|e\rangle + c_g|g\rangle$ with $|c_e|^2 + |c_g|^2 = 1$ at a single atomic site, by using the stimulated Raman adiabatic passage (STIRAP) technique [25]. This kind of pure state may be formed by time-overlapping excitation pulses of two frequencies, $\approx\epsilon_{pe}$ and $\approx\epsilon_{pg}$. The state is a so-called dark state because no emission from $|p\rangle$ is observed despite irradiation capable of making both transitions, $|p\rangle \rightarrow |e\rangle$ and $|p\rangle \rightarrow |g\rangle$.

The medium polarization r_i in the dark state is given by

$$r_1 = 2\sqrt{p(1-p)}\cos\theta_0, \quad r_2 = 2\sqrt{p(1-p)}\sin\theta_0, \quad r_3 = 2p - 1, \tag{24}$$

with p the fraction in state $|e\rangle$. When this type of initial polarization of the dark state is formed, one may expect to expedite the coherence development for PSR, as shown in the following section. When a cw laser is used for the trigger, two overlapping pulses may induce PSR at the same time when the emission from $|p\rangle$ disappears: thus it may be called PSR from the dark.

IV. NUMERICAL SOLUTIONS FOR A HIGH-DENSITY TARGET WITH INITIAL COHERENCE

We first comment on what the number density n of a target precisely means. This is the total number of atoms or molecules per a unit volume participating in PSR phenomena; hence it is the added sum of the densities in states $|e\rangle$ and $|g\rangle$. Note also that state $|g\rangle$ may or may not be the ground state of the atoms or molecules. For instance, in the p-H_2 transition $X^1\Sigma_g^+ v = 2 \rightarrow 1$, the target number density n may be much less than the ground-state number density since $|g\rangle = (Xv = 1)$ is also an excited state.

The time evolution from a dark state with an initial polarization value given by Eq. (24) is illustrated for a p-H_2 number density of 1×10^{21} cm^{-3} in Figs. 3–11. We show dependence of the symmetric output pulse on the trigger power in the range of 10^{-12}–1 W mm^{-2} for $n = 1 \times 10^{21}$ cm^{-3} in Fig. 3, which demonstrates two important features of explosive PSR with large initial coherence: (1) the highest peak of PSR output is almost independent of the trigger power, suggesting a sudden, macroscopic release of energy (its density is $\approx\epsilon_{eg}n$) stored between two levels, $|e\rangle$ and $|g\rangle$, and (2) the onset time of explosive events, which may be called the delay time, depends on the input trigger power very weakly, and a

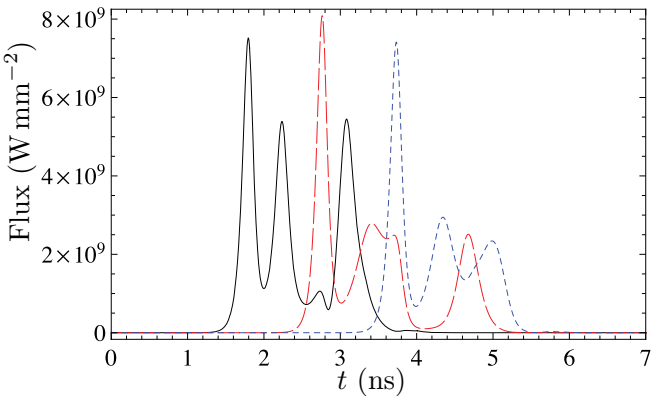

FIG. 3. (Color online) Trigger power dependence of time-evolving output flux from the symmetric trigger irradiation of the power range, 10^{-12} to 1 W mm^{-2}, under the conditions of $n = 1 \times 10^{21}$ cm^{-3}, target length of 30 cm, relaxation times $T_2 = 10$ ns and $T_1 = 10^3$ ns, and the initial polarization $r_1 = 1, r_2 = r_3 = 0$. Depicted outputs from 1 W mm^{-2} (solid black line), 10^{-6} W mm^{-2} (long-dashed red line), and 10^{-12} W mm^{-2} (short-dashed blue line) trigger power are displaced almost equidistantly in the first peak positions. Transition $Xv = 1 \rightarrow Xv = 0$ of p-H_2 is considered. About 70% of the stored energy in the initial metastable state is released in these cases.

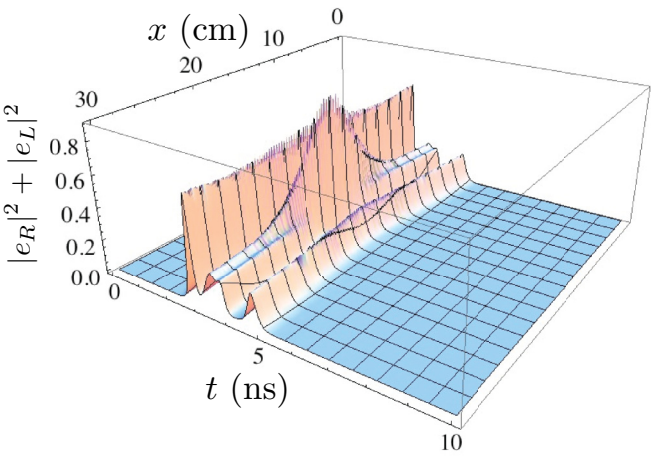

FIG. 4. (Color online) Space-time profile of dimensionless field energy $|e_R|^2 + |e_L|^2$ for the 1 μW mm^{-2} case of Fig. 3.

linear logarithmic dependence has been confirmed up to 1 pW mm^{-2} (instantaneous enhancement factor of $\sim 8 \times 10^{21}$ in this case). A similar logarithmic power dependence of the delay time has been observed in numerical simulations of the single-photon superradiance when the system is subjected to the trigger.

The integrated flux is $\sim |E_{\max}|^2 \Delta t$, where Δt is the time width of the explosive event. $|E_{\max}|^2 = O(\epsilon_{eg} n)$, and this integrated flux is estimated as $O(1/\mu_{ge})$, a quantity that is independent of the target number density n, if the explosive event occurs. These figures, Figs. 3–13 show dramatic effects of the initial coherence of the dark state. Observation of explosive events requires a target length $\gg 1/\alpha_m \propto 1/n$. The detailed time structure of pulses as observed in Fig. 3 may differ if one adopts different available experimental parameters, but the output release of the energy flux of order $\epsilon_{eg} n$ is universal in explosive PSR events.

The spatial profiles of field fluxes and polarization components r_i within the target are illustrated in Figs. 4–11. In this parameter set, about $\sim$30% of the stored energy $\epsilon_{eg} n$ [the

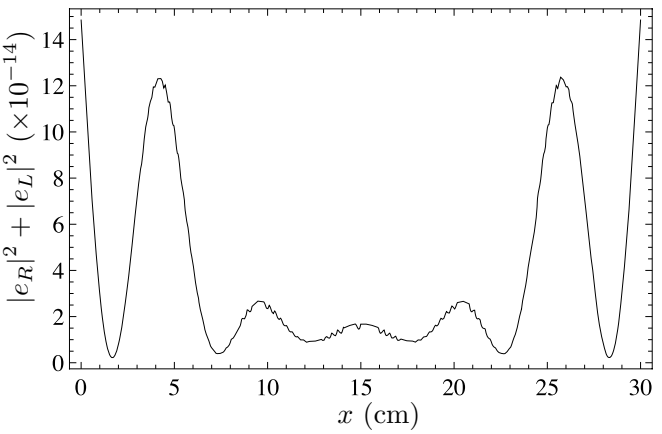

FIG. 5. Spatial profile at the latest time, 10 ns after trigger irradiation, of Fig. 4. Note the large reduction by $O(10^{-13})$ in the power scale.

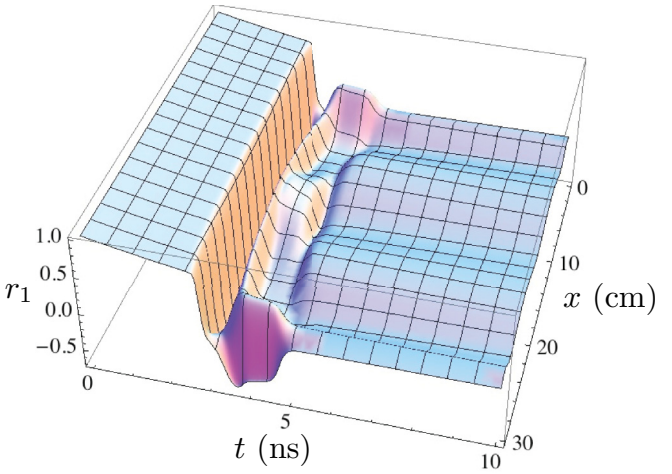

FIG. 6. (Color online) Space-time profile of r_1 for the 1 μW mm^{-2} case of Fig. 3.

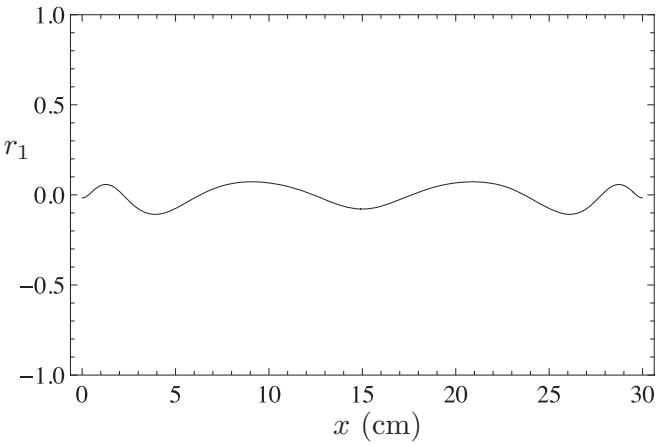

FIG. 7. Spatial profile of r_1 at the latest time, 10 ns after trigger irradiation, of Fig. 6.

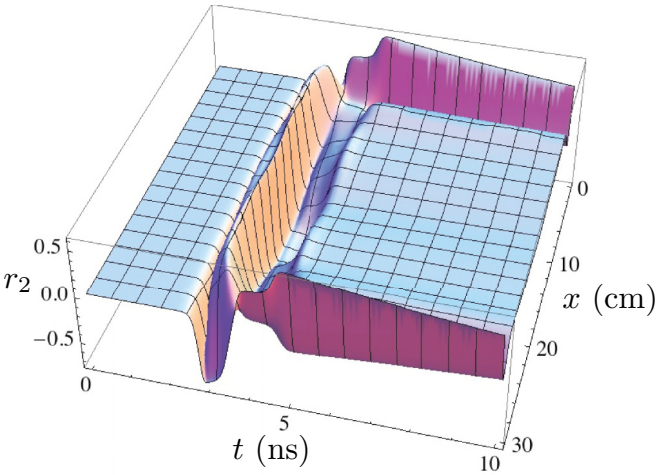

FIG. 8. (Color online) Space-time profile of r_2 for the 1 μW mm^{-2} case of Fig. 3.

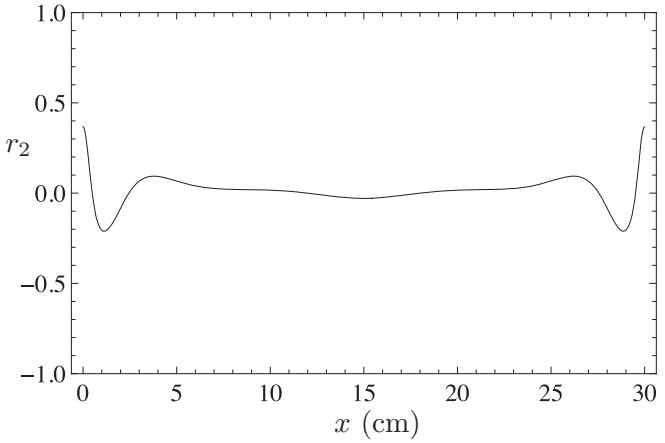

FIG. 9. Spatial profile of r_2 at the latest time, 10 ns after trigger irradiation, of Fig. 8.

corresponding flux unit being 1.2×10^9 W mm^{-2} ($n/10^{21}$ cm^{-3})] still remains in the target long after explosive PSR, and we observe a seemingly stable target state. Note that dimensionless fields $|e_i|^2 = |E_i|^2/(\epsilon_{eg} n)$ are plotted in Figs. 4 and 5.

The result for a solid density of $n = 2.6 \times 10^{22}$cm^{-3} and a smaller excitation of $r_3 \approx -1$ is shown in Fig. 12. There is a threshold of the excitation fraction of $|e\rangle$, located between 0.2% and 0.5%, above which dramatic explosive PSRs emerge, as inferred from comparison of the two plots in Fig. 12.

So far we have mostly showed explosive outputs in which most of the stored energy between $|e\rangle$ and $|g\rangle$ is released during time span <10 ns after the time delay. There is, however, a linear regime under a large initial coherence $r_i, i = 1,2$, in which the output flux is amplified in proportion to the trigger power. For instance, the amplification factor is $\sim 10^2$ in the trigger power range of 1 μW mm^{-2} to 1 W mm^{-2} for the three different choices of initial r_i values in Fig. 13. In Fig. 13 we show the output fluxes in the linear regime taking as an example a trigger power of 1 mW mm^{-2}. Although not shown in Fig. 13, the linearity of the output power to the trigger power has been checked for this set of parameters.

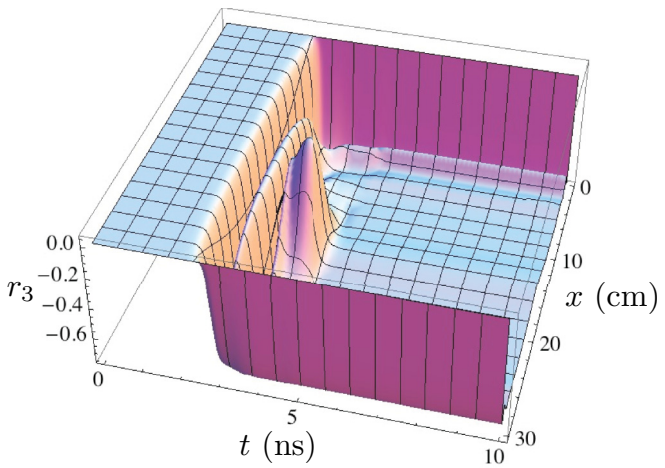

FIG. 10. (Color online) Space-time profile of r_3 for the 1 μW mm^{-2} case of Fig. 3.

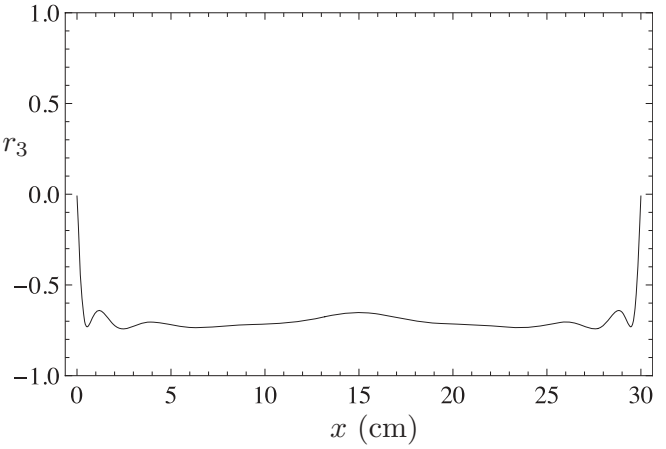

FIG. 11. Spatial profile of r_3 at the latest time, 10 ns after trigger irradiation, of Fig. 10.

V. STATIC REMNANT AND SPINORIAL SOLITONS

In addition to the dramatic explosive PSR emission it is also important to watch the remnants after the PSR emission since previous Figs. 5, 7, 9, and 11 at the latest times may be taken to suggest the formation of objects of nontrivial spatial profiles. Let us derive for this purpose the asymptotic form of fundamental equations. We anticipate that both the medium polarization $\vec{r}$ and fields e_R, e_L change little with time in the time region of $t \gg 1/\alpha_m$ after PSR emission. By taking vanishing time derivatives, one may eliminate polarizations r_i in favor of field components and write profile equations of spatial variation for fields,

$$e_R' = 2ige_R + ife_L^*, \quad e_L' = -2ige_L - ife_R^*, \tag{25}$$

$$g = g(e_R, e_L) = \gamma_+ - \gamma_- \frac{16\gamma_-^2\tau_2^2(|e_R|^2 + |e_L|^2)^2 + 1}{16\gamma_-^2\tau_2^2(|e_R|^2 + |e_L|^2)^2 + 64\tau_1\tau_2|e_R e_L|^2 + 1}, \tag{26}$$

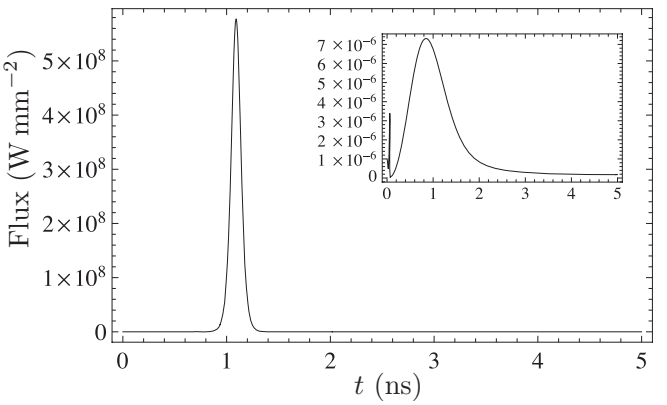

FIG. 12. Output flux for the solid target number density of 2.6×10^{22} cm^{-3} with a length of 2 cm, trigger power of 1 μW mm^{-2}, relaxation times $T_2 = 10$ ns and $T_1 = 10^3$ ns, and a smaller population $r_3 = -0.99$ (0.5% excitation) [$r_3 = -0.996$ (0.2% excitation) in the inset]. The other initial components are taken as $r_1 = \sqrt{1 - r_3^2}$, $r_2 = 0$. Note the large flux scale difference of $\sim 10^{14}$ in the two plots.

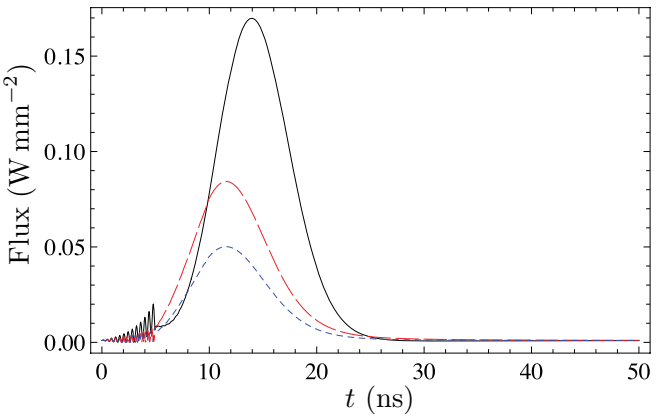

FIG. 13. (Color online) Output flux of weak p-H_2 PSR in the linear regime in which the output power is $O(\sim 10^2)$ times the trigger power for initial $(r_3,r_1,r_2) = (0,1,0)$ (solid black line), $(1/\sqrt{2},1/\sqrt{2},0)$ (long-dashed red line), and $(-1/\sqrt{2},1/\sqrt{2},0)$ (short-dashed blue line), using the same set of other parameters: $n = 1 \times 10^{20}$ cm^{-3}, target length of 1.5 m, relaxation times $T_2 = 10$ ns and $T_1 = 10^3$ ns, and trigger power of 1 mW mm^{-2}. The output power scales with the trigger power, as explicitly checked in the range of 1 μW mm^{-2} to 1 W mm^{-2}.

$$f = f(e_R,e_L) = \frac{4\tau_2 e_R e_L((4\gamma_-\tau_2(|e_R|^2+|e_L|^2)-i)}{16\gamma_-^2\tau_2^2(|e_R|^2+|e_L|^2)^2+64\tau_1\tau_2|e_Re_L|^2+1}, \quad (27)$$

$$r_3 = -\frac{16\gamma_-^2\tau_2^2(|e_R|^2+|e_L|^2)^2+1}{16\gamma_-^2\tau_2^2(|e_R|^2+|e_L|^2)^2+64\tau_1\tau_2|e_Re_L|^2+1}, \quad (28)$$

where a prime indicates the spatial derivative ∂_ξ.

Despite the complicated field-dependent coefficient functions that appear in f and g, the structure of profile equation (25) is rather simple. Oscillatory behavior governed by terms $\propto g$ can be eliminated by taking three bilinear forms of fields, $|e_R|^2, |e_L|^2$, and e_Re_L:

$$(|e_R|^2+|e_L|^2)' = 0, \quad (|e_R|^2-|e_L|^2)' = -4\mathrm{Im}(f e_R^* e_L^*), \quad (e_Re_L)' = -if(|e_R|^2-|e_L|^2), \quad (29)$$

where the function f depends effectively on e_Re_L alone since the total flux is a constant of integration due to the first equation of Eq. (29); hence with a real constant e_0, $|e_R(\xi)|^2+|e_L(\xi)|^2 = e_0^2$. The set of profile equations, (29), is transformed into two equations of the phase functions, $\varphi(\xi)$ and $S(\xi)$, defined by

$$e_R(\xi) = e_0\cos\varphi(\xi), \quad e_L(\xi) = e_0 e^{iS(\xi)}\sin\varphi(\xi), \quad (30)$$

$$\varphi' = \frac{2e_0^2\tau_2}{1+16\gamma_-^2e_0^4\tau_2^2+16e_0^4\tau_1\tau_2\sin^2(2\varphi)}\sin(2\varphi), \quad (31)$$

$$S' = \frac{16\gamma_-e_0^2\tau_2^2}{1+16\gamma_-^2e_0^4\tau_2^2+16e_0^4\tau_1\tau_2\sin^2(2\varphi)}\cos(2\varphi), \quad (32)$$

with $\varphi(l/2) = \pi/4, S(l/2) = 0, l = \alpha_m L$. Since the e_i's contain four real functions, the resulting two equations here reflect a nontrivial self-consistency of the ansatz (30). A similar equation with $R \leftrightarrow L$ interchanged may be set up, suggesting another kind of soliton.

The equation for the angle function $\varphi(\xi)$ [(31)] is self-contained and has the following analytic solution under the boundary condition $e_R(l/2) = e_0/\sqrt{2}$:

$$2e_R^2 - e_0^2 + \frac{16\gamma_-^2\tau_2^2e_0^4+1}{32\tau_1\tau_2e_0^4}\ln\frac{e_R^2}{e_0^2-e_R^2} = -\frac{\xi-l/2}{4\tau_1}. \quad (33)$$

The field may decrease exponentially in the central region, as $e_R^2 \propto \exp[-8\tau_2e_0^4|\xi-l/2|/(16\gamma_-^2\tau_2^2e_0^4+1)]$. One may define the soliton size by the e-folding factor as $\xi_s = (16\gamma_-^2\tau_2^2e_0^4+1)/(8\tau_2e_0^4)$. The actual soliton size is $x_s = \xi_s/\alpha_m$.

The spatial variation of $e_R \propto \cos\varphi(\xi)$ is monotonic, decreasing or increasing depending on the φ region of either $[0,\pi/2]$ or $[\pi/2,\pi]$ (defined modulo π). These two fundamental regions are separated since $\varphi' = 0$ at the edges of these regions because $\sin(2\varphi) = 0$ there. One may identify these two solutions as different objects. Either of the fields e_R and e_L vanishes at the edges of fundamental regions, but not both. The solution defined by the fundamental region $[0,\pi/2]$ corresponds to an absorber soliton in which both R and L fluxes are absorbed at edges but are not emitted at the other edges, as illustrated in Figs. 14 and 15. This object may be called the absorber soliton. The other fundamental region $[\pi/2,\pi]$ gives

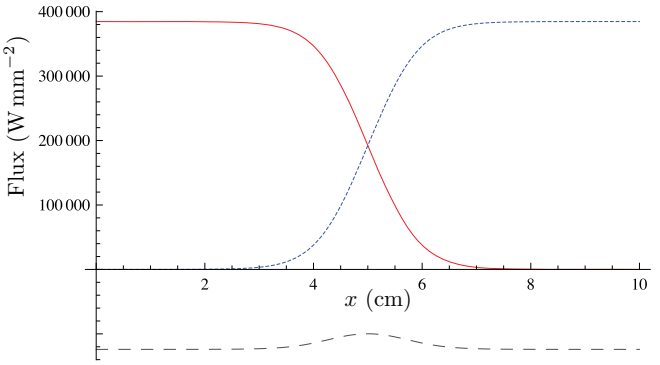

FIG. 14. (Color online) Profile of fields and r_3 of the helical absorber soliton. $|E_R|^2$ (solid red line) and $|E_L|^2$ (short-dashed blue line; both in units of W mm^{-2}) and r_3 (long-dashed black line; in arbitrary units) are plotted for the case of $n = 2.6 \times 10^{22}$ cm^{-3}, $T_2 = 20$ ns, $T_1 = 10^3$ ns, and $r_3 \approx -1$ near the edges and $r_3 \approx -0.8$ in the middle.

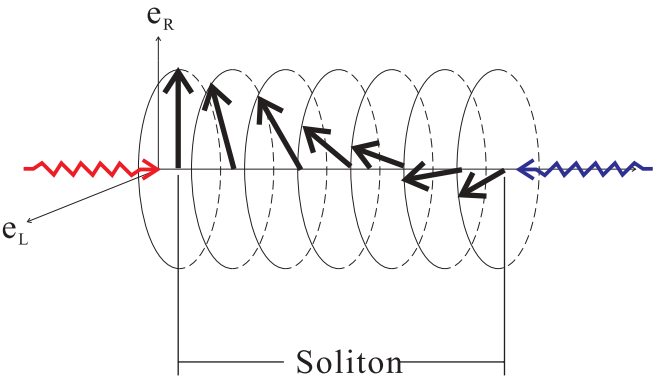

FIG. 15. (Color online) Helical structure of the absorber soliton. The target region is irradiated from both ends by trigger lasers of different colors. $\vec{X}(\xi) = (\cos\varphi, \cos S\sin\varphi, \sin S\sin\varphi)$, with φ and S defined by Eq. (30), may wind. In the return trip from the right edge to the left edge (not shown here), $\vec{X}(\xi)$ further winds and comes back with $\vec{X}(\pi) = -\vec{X}(0)$ at the left edge, giving a spinor field. This is an absorber soliton without emission at two ends.

an emitter soliton which may be realized when the excited $|e\rangle$ state is sufficiently occupied. The existence of two types of soliton condensates is an important result, indicating the existence of a new kind of topological soliton whose topology is discussed in Appendix C.

When the target size L is large and $L \gg \xi_s/\alpha_m$, one may expect a copious production of absorbers and emitters within the target. When the target size is smaller than ξ_s/α_m, the target edge effect becomes important (in general, destroying solitons, or blocking their formation), and it may be difficult to create a soliton.

The soliton solution obtained by direct numerical integration of Eq. (31) is illustrated in Fig. 14 along with the distribution of the population difference r_3. Solitons are characterized by two end points of $r_3 \approx -1$ and an intermediate region of $r_3 \approx 0$. It is important to have a long enough target to accommodate many solitons within the target. The soliton size can be made smaller if one can use a larger target number density close to the solid density.

VI. CONCLUSION

In summary, we derived and numerically solved the master equation for the time evolution of PSR emission and the formation of field condensates in long, dense targets. We have demonstrated (1) numerical identification of two different types of PSR events, explosive and weak ones, and (2) the theoretical existence of spinorial solitons that are stable against PSR emission. Realistic experiments can be designed using numerical solutions of our master equation.

Note added. Recently, we became aware of a related work [26] where the time evolution of triggered two-photon coherence is examined. The authors of Ref. [26] treat the field differently from the one of our semiclassical approach. Our approach gives very short coherence development time on the order of several nanoseconds in dense targets.

ACKNOWLEDGMENTS

This research was partially supported by Grant-in-Aid for Scientific Research on Innovative Areas "Extreme quantum world opened up by atoms" (21104002) from the Ministry of Education, Culture, Sports, Science, and Technology of Japan.

APPENDIX A: TWO-LEVEL EFFECTIVE MODEL INTERACTING WITH MULTIMODE FIELDS

We extend the results of Appendix A in Ref. [14] to the case of multimode fields such that the two-color problem including the propagation effect is properly treated. This is the most general case of the two-photon problem. Its notation in this work is slightly changed.

1. Atomic system

The state vector of an atom can be expanded in terms of the wave function,

$$|\psi(t)\rangle = c_g(t)e^{-i\epsilon_g t}|g\rangle + c_e(t)e^{-i\epsilon_e t}|e\rangle + \sum_p c_p(t)e^{-i\epsilon_p t}|p\rangle\,. \tag{A1}$$

The $c_a(t)$'s are probability amplitudes in an interaction picture where ϵ_a's are energies of atomic states. The atomic system may interact with light fields. The electric field $E(x,t)$ that appears in the Hamiltonian via $E1$ or $M1$ transition is assumed to have one vector component alone; that is, we ignore the effects of field polarization. This is a valid approach under a number of circumstances. We then decompose the real field variable $E(x,t)$ into a Fourier series, $e^{-i\omega_j t}$ times a complex envelope amplitude $E_j(x,t)$, and its conjugate, where $E_j(x,t)$ is assumed to be slowly varying in time,

$$E(x,t) = \sum_j [E_j^*(x,t)e^{i\omega_j t} + E_j(x,t)e^{-i\omega_j t}]. \tag{A2}$$

Each discrete mode j is taken to be independent. The most interesting cases are those of two modes with $\omega_1 + \omega_2 = \epsilon_{eg}$ and the single mode with $\omega = \epsilon_{eg}/2$.

The Schrödinger equation for a single atom,

$$i\frac{\partial}{\partial t}|\psi(t)\rangle = (H_0 + dE)|\psi(t)\rangle, \tag{A3}$$

where H_0 is the atomic Hamiltonian, is used to derive the upper level amplitude $c_p(t)$. Using

$$i\frac{\partial}{\partial t}\langle p|\psi(t)\rangle = \langle p|(H_0 + dE)|\psi(t)\rangle, \tag{A4}$$

we have

$$i\frac{dc_p}{dt}e^{-i\epsilon_p t} = (d_{pe}c_e e^{-i\epsilon_e t} + d_{pg}c_g e^{-i\epsilon_g t})E, \tag{A5}$$

where d_{ab} are dipole matrix elements. This can formally be integrated to

$$\begin{aligned} c_p(t) &= -i\int_0^t dt'[d_{pe}c_e(t')e^{i\epsilon_{pe}t'} + d_{pg}c_g(t')e^{i\epsilon_{pg}t'}]E(x,t') \\ &= -i\int_0^t dt' \sum_j [d_{pe}c_e(t')e^{i\epsilon_{pe}t'} + d_{pg}c_g(t')e^{i\epsilon_{pg}t'}] \\ &\quad \times [E_j^*(x,t')e^{i\omega_j t'} + E_j(x,t')e^{-i\omega_j t'}], \end{aligned} \tag{A6}$$

with $\epsilon_{ab} = \epsilon_a - \epsilon_b$ being the atomic level energy difference. The initial condition $c_p(0) = 0$ is assumed here.

2. Markovian approximation and effective two-level model

The basic strategy of deriving equations for the lower two-level amplitudes c_e and c_g in a closed form is to eliminate atomic variables c_p's related to the upper levels. This is essentially done by neglecting a long-time memory effect (the Markovian approximation) and making a slowly varying envelope approximation (SVEA). The idea of the Markovian approximation is to replace dynamical variables, $c_e(t'), c_g(t')$, and $E_j(x,t')$ in the integrand of Eq. (A6), by their values at time t, neglecting all the past memory effects.

This gives

$$c_p(t) \approx \sum_j d_{pe}c_e\left(\frac{1-e^{i(\omega_j+\epsilon_{pe})t}}{\omega_j+\epsilon_{pe}}E_j^* - \frac{1-e^{-i(\omega_j-\epsilon_{pe})t}}{\omega_j-\epsilon_{pe}}E_j\right) + d_{pg}c_g\left(\frac{1-e^{i(\omega_j+\epsilon_{pg})t}}{\omega_j+\epsilon_{pg}}E_j^* - \frac{1-e^{-i(\omega_j-\epsilon_{pg})t}}{\omega_j-\epsilon_{pg}}E_j\right), \quad \text{(A7)}$$

which is inserted into equations for the lower levels,

$$\frac{dc_e}{dt} = -i\sum_p d_{ep}E(x,t)c_p(t)e^{-i\epsilon_{pe}t}, \quad \text{(A8)}$$

$$\frac{dc_g}{dt} = -i\sum_p d_{gp}E(x,t)c_p(t)e^{-i\epsilon_{pg}t}. \quad \text{(A9)}$$

Note that $d_{ab} = d_{ba}$ are real by an appropriate choice of phases.

We ignore rapidly oscillating terms, keeping in mind the two most important cases of the mode choice. The result is

$$\frac{d}{dt}\begin{pmatrix} c_e \\ c_g \end{pmatrix} = -i\mathcal{H}_I\begin{pmatrix} c_e \\ c_g \end{pmatrix}, \quad \text{(A10)}$$

$$-\mathcal{H}_I = \sum_{jj'}\begin{pmatrix} \mu_{ee}(\omega_j,\omega_{j'})e^{i(\omega_j-\omega_{j'})t}E_j^*E_{j'} & e^{-i(\omega_j+\omega_{j'}-\epsilon_{eg})t}\mu_{eg}(\omega_j,\omega_{j'})E_jE_{j'} \\ e^{i(\omega_j+\omega_{j'}-\epsilon_{eg})t}\mu_{ge}(\omega_j,\omega_{j'})E_j^*E_{j'}^* & \mu_{gg}(\omega_j,\omega_{j'})e^{i(\omega_j-\omega_{j'}t)}E_j^*E_{j'} \end{pmatrix} \equiv \mathcal{E}_j\mathcal{M}_{jj'}\mathcal{E}_{j'}, \quad \text{(A11)}$$

$$\mu_{ee}(\omega_j,\omega_{j'}) = \sum_p \frac{d_{pe}^2(2\epsilon_{pe}+\omega_j-\omega_{j'})}{(\epsilon_{pe}+\omega_j)(\epsilon_{pe}-\omega_{j'})}, \quad \mu_{gg}(\omega_j,\omega_{j'}) = \sum_p \frac{d_{pg}^2(2\epsilon_{pg}+\omega_j-\omega_{j'})}{(\epsilon_{pg}+\omega_j)(\epsilon_{pg}-\omega_{j'})}, \quad \text{(A12)}$$

$$\mu_{eg}(\omega_j,\omega_{j'}) = \sum_p \frac{d_{pe}d_{pg}[\epsilon_{pg}-(\omega_j+\omega_{j'})/2]}{(\epsilon_{pg}-\omega_j)(\epsilon_{pg}-\omega_{j'})}, \quad \mu_{ge}(\omega_j,\omega_{j'}) = \sum_p \frac{d_{pe}d_{pg}[\epsilon_{pe}+(\omega_j+\omega_{j'})/2]}{(\epsilon_{pe}+\omega_j)(\epsilon_{pe}+\omega_{j'})}. \quad \text{(A13)}$$

$\mathcal{E}$ may contain both E_j and E_j^*. We simplify the notation below such that fields are redefined incorporating oscillating factors $e^{-i\omega_j t}$ in E_j^+ and so on.

3. Single-color problem

We apply the result to the problem of counterpropagating fields E_R and E_L of a single color of $\omega_0 = \epsilon_{eg}/2$. In the 2×2 Hamiltonian, (A11), one may use the complex field $E^+ \equiv E_j e^{-i\omega_j t}$ (the positive energy component corresponding to the photon annihilation operator) and its conjugate $E^- \equiv E_j^* e^{i\omega_j t}$ (the negative energy component corresponding to the photon creation operator) to eliminate phase factors except $e^{\pm i\epsilon_{eg}t}$, as done in the main text. Since each mode is independent, it separately satisfies the field commutation relation, which is necessary to derive the quantum field equation, justifying the result for the case of $\omega = \omega_0 = \epsilon_{eg}/2$.

More concretely,

$$-\mathcal{H}_I = \begin{pmatrix} \mu_{ee}(E_R^+E_R^- + E_L^+E_L^- + E_R^+E_L^- + E_L^+E_R^-) & e^{i\epsilon_{eg}t}\mu_{ge}(E_R^+E_R^+ + E_L^+E_L^+ + 2E_R^+E_L^+) \\ e^{-i\epsilon_{eg}t}\mu_{ge}(E_R^-E_R^- + E_L^-E_L^- + 2E_R^-E_L^-) & \mu_{gg}(E_R^+E_R^- + E_L^+E_L^- + E_R^+E_L^- + E_L^+E_R^-) \end{pmatrix}, \quad \text{(A14)}$$

$$\mu_{ge} = \frac{2d_{pe}d_{pg}}{\epsilon_{pg}+\epsilon_{pe}}, \quad \mu_{aa} = \frac{2d_{pa}^2\epsilon_{pa}}{\epsilon_{pa}^2-\omega_0^2}. \quad \text{(A15)}$$

(RR) and (LL) terms describe pulse propagation with compression and splitting, while (RL) terms describe backscattering, pair creation, and pair annihilation.

4. Two-color problem

We may consider for E_R and E_L envelopes of two different colors of ω_i with $\omega_1+\omega_2 = \epsilon_{eg}$. The separation of the cross-mode terms leads to

$$\mathcal{H}_I = \mathcal{H}_{d,R} + \mathcal{H}_{d,L} + \mathcal{H}_{12,R} + \mathcal{H}_{12,L} + \mathcal{H}_{12,RL}, \quad \text{(A16)}$$

$$-\mathcal{H}_{d,i} = \begin{pmatrix} \sum_{i,a}\mu_{ee}(\omega_a,\omega_a)E_{i,a}^+E_{i,a}^- & e^{i\epsilon_{eg}t}\sum_{i,a}\mu_{eg}(\omega_a,\omega_a)E_{i,a}^+E_{i,a}^+ \\ e^{-i\epsilon_{eg}t}\sum_{i,a}\mu_{ge}(\omega_a,\omega_a)E_{i,a}^-E_{i,a}^- & \sum_{i,a}\mu_{gg}(\omega_a,\omega_a)E_{i,a}^+E_{i,a}^- \end{pmatrix}, \quad \text{(A17)}$$

$$-\mathcal{H}_{12,i} = \begin{pmatrix} \mu_{ee}(\omega_1,\omega_2)E_{i,1}^+E_{i,2}^- + \mu_{ee}(\omega_2,\omega_1)E_{i,2}^+E_{i,1}^- & e^{i\epsilon_{eg}t}2\mu_{eg}(\omega_1,\omega_2)E_{i,1}^+E_{i,2}^+ \\ e^{-i\epsilon_{eg}t}2\mu_{ge}(\omega_1,\omega_2)E_{i,1}^-E_{i,2}^- & \mu_{gg}(\omega_1,\omega_2)E_{i,1}^+E_{i,2}^- + \mu_{gg}(\omega_2,\omega_1)E_{i,2}^+E_{i,1}^- \end{pmatrix}, \quad \text{(A18)}$$

$$-(\mathcal{H}_{12,RL})_{aa} = \mu_{aa}(\omega_1,\omega_2)E^+_{R,1}E^-_{L,2} + \mu_{aa}(\omega_2,\omega_1)E^+_{R,2}E^-_{L,1} + \mu_{aa}(\omega_1,\omega_2)E^+_{L,1}E^-_{R,2} + \mu_{aa}(\omega_2,\omega_1)E^+_{L,2}E^-_{R,1}, \tag{A19}$$

$$-(\mathcal{H}_{12,RL})_{eg} = e^{i\epsilon_{eg}t}2\mu_{eg}(\omega_1,\omega_2)(E^+_{R,1}E^+_{L,2} + E^+_{R,2}E^+_{L,1}), \tag{A20}$$

$$\mu_{aa}(\omega_1,\omega_2) = \frac{d^2_{pa}(2\epsilon_{pa}+\omega_1-\omega_2)}{(\epsilon_{pa}+\omega_1)(\epsilon_{pa}-\omega_2)}, \tag{A21}$$

$$\mu_{ge}(\omega,\epsilon_{eg}-\omega) = \mu_{ge}(\epsilon_{eg}-\omega,\omega) = \mu_{eg}(\omega,\epsilon_{eg}-\omega) = \mu_{eg}(\epsilon_{eg}-\omega,\omega) = \frac{d_{pe}d_{pg}(\epsilon_{pg}+\epsilon_{pe})}{(\epsilon_{pe}+\omega)(\epsilon_{pg}-\omega)}\,. \tag{A22}$$

5. Bloch equation

The Bloch vector defined by

$$\vec{R} = \langle\psi|\vec{\sigma}|\psi\rangle = \mathrm{tr}\,\vec{\sigma}\,\rho, \qquad \rho = |\psi\rangle\langle\psi| = \begin{pmatrix} c^*_e c_e & c^*_e c_g \\ c^*_g c_e & c^*_g c_g \end{pmatrix}, \tag{A23}$$

satisfies the quantum-mechanical equation (disregarding relaxation terms) $\partial_t\vec{R} = -i\,\mathrm{tr}\,\vec{\sigma}[\mathcal{H}_I,\rho]$. Explicit calculation using the Hamiltonian above gives

$$\partial_t R_1 = (\mu_{ee}-\mu_{gg})E^+E^-R_2 - i\mu_{ge}(e^{i\epsilon_{eg}t}E^+E^+ - e^{-i\epsilon_{eg}t}E^-E^-)R_3, \tag{A24}$$

$$\partial_t R_2 = -(\mu_{ee}-\mu_{gg})E^+E^-R_1 + \mu_{ge}(e^{i\epsilon_{eg}t}E^+E^+ + e^{-i\epsilon_{eg}t}E^-E^-)R_3, \tag{A25}$$

$$\partial_t R_3 = \mu_{ge}[i(e^{i\epsilon_{eg}t}E^+E^+ - e^{-i\epsilon_{eg}t}E^-E^-)R_1 - (e^{i\epsilon_{eg}t}E^+E^+ + e^{-i\epsilon_{eg}t}E^-E^-)R_2]. \tag{A26}$$

We suppressed mode index j for simplicity. The conservation law holds: $\partial_t(R_1^2+R_2^2+R_3^2) = 0$.

6. Field equation

The commutation relation of fields necessary to derive the quantum field equation $[E_y(\vec{r},t),B_z(\vec{r}\,',t)] = i\partial_x\delta^3(\vec{r}-\vec{r}\,')$ is valid for each independent mode. The double commutator,

$$\partial_t^2\vec{E}^{\pm} = -[\![H,[H,\vec{E}^{\pm}]\!]\!], \qquad H = \int d^3x(\mathcal{H}_f + \mathrm{tr}\,\rho\mathcal{H}_I), \tag{A27}$$

$$\mathrm{tr}\,\rho\mathcal{H}_I = \langle\psi|\mathcal{H}|\psi\rangle = -(\mu_{ee}|c_e|^2 + \mu_{gg}|c_g|^2)E^+E^- - \mu_{ge}(c^*_e c_g E^+E^+ + c^*_g c_e E^-E^-), \tag{A28}$$

with the field energy density $\mathcal{H}_f = (\vec{E}^2+\vec{B}^2)/2$, is calculated as

$$\left(\partial_t^2 - \vec{\nabla}^2\right)\vec{E}^{\pm}_j = \vec{\nabla}^2(\mathcal{D}_{jj'}\vec{E}_{j'})^{\pm}, \tag{A29}$$

$$-\mathcal{D}_{jj'}\vec{E}^+_{j'} = \left(\frac{(\mu_{ee}+\mu_{gg})_{jj'}}{2}n + \frac{(\mu_{ee}-\mu_{gg})_{jj'}}{2}R_3\right)\vec{E}^+_{j'} + (\mu_{ge})_{jj'}e^{-i\epsilon_{eg}t}(R_1 - iR_2)\vec{E}^-_{j'}\,. \tag{A30}$$

7. SVEA and dimensionless equations for two-color modes

All terms in both the Bloch and field equations must have the same oscillatory behavior for global evolution of polarization and fields. This gives a phase-matching condition of the form $\omega_1+\omega_2 = \epsilon_{eg}$ and momentum balance with $E_R \propto e^{i\omega x}, E_L \propto e^{-i\omega x}$. For time SVEA one may then eliminate the phase factor $e^{\pm i\epsilon_{eg}t}$ in the Bloch equation. For space SVEA we introduce spatial variation of polarization of the form

$$R_i = R_i^{(0)} + R_i^{(+)}e^{2i\omega x} + R_i^{(-)}e^{-2i\omega x}\,. \tag{A31}$$

The left-hand side of the field equations is $-2i\omega(\partial_t \pm \partial_x)E_{R,L}$ for the counterpropagating modes of the same frequency; hence (with $\partial_\pm \equiv \partial_t \pm \partial_x$)

$$\partial_+E_R = \frac{i\omega}{2}\left[\left(\frac{\mu_{ee}+\mu_{gg}}{2}n + \frac{\mu_{ee}-\mu_{gg}}{2}R_3^{(0)}\right)E_R + \frac{\mu_{ee}-\mu_{gg}}{2}R_3^{(+)}E_L + \mu_{ge}[(R_1-iR_2)^{(0)}E_L^* + (R_1-iR_2)^{(+)}E_R^*]\right], \tag{A32}$$

$$\partial_-E_L = \frac{i\omega}{2}\left[\left(\frac{\mu_{ee}+\mu_{gg}}{2}n + \frac{\mu_{ee}-\mu_{gg}}{2}R_3^{(0)}\right)E_L + \frac{\mu_{ee}-\mu_{gg}}{2}R_3^{(-)}E_R + \mu_{ge}[(R_1-iR_2)^{(0)}E_R^* + (R_1-iR_2)^{(-)}E_L^*]\right]. \tag{A33}$$

We introduce the dimensionless unit:

$$(\xi,\tau)=(\alpha_m x,\alpha_m t),\quad \alpha_m(\omega)=\frac{\epsilon_{eg}}{2}n\mu_{ge}(\omega,\epsilon_{eg}-\omega),\quad \left|e_{L,R}^{(1),(2)}\right|^2=\frac{\left|E_{L,R}^{(1),(2)}\right|^2}{\epsilon_{eg}n},\quad r_i=\frac{R_i}{n}. \tag{A34}$$

Assume an R mover of frequency ω_1 and an L mover of frequency ω_2 (but not an R mover of frequency ω_2 and an L mover of frequency ω_1). Note the universal parameter $\mu_{eg}(\omega_1,\omega_2)=\mu_{ge}(\omega_1,\omega_2)$ for any combination of $\omega_1+\omega_2=\epsilon_{eg}$. The master equations for medium polarization and fields are

$$\begin{aligned}\partial_\tau r_1^{(0)}&=4(\gamma_-^{(1)}|e_R|^2+\gamma_-^{(2)}|e_L|^2)r_2^{(0)}+8\mathrm{Im}(e_Re_L)r_3^{(0)}+4\gamma_-^{(12)}e_Re_L^*r_2^{(-)}+4\gamma_-^{(21)}e_Le_R^*r_2^{(+)}\\&\quad-2i\left[e_L^2-(e_R^*)^2\right]r_3^{(+)}-2i\left[e_R^2-(e_L^*)^2\right]r_3^{(-)}-\frac{r_1^{(0)}}{\tau_2},\end{aligned} \tag{A35}$$

$$\partial_\tau r_1^{(+)}=4\gamma_-^{(12)}e_Re_L^*r_2^{(0)}-2i\left[e_R^2-(e_L^*)^2\right]r_3^{(0)}+4(\gamma_-^{(1)}|e_R|^2+\gamma_-^{(2)}|e_L|^2)r_2^{(+)}+8\mathrm{Im}(e_Re_L)r_3^{(+)}-\frac{r_1^{(+)}}{\tau_2}, \tag{A36}$$

$$\begin{aligned}\partial_\tau r_2^{(0)}&=-4(\gamma_-^{(1)}|e_R|^2+\gamma_-^{(2)}|e_L|^2)r_1^{(0)}+8\mathrm{Re}(e_Re_L)r_3^{(0)}-4\gamma_-^{(12)}e_Re_L^*r_1^{(-)}-4\gamma_-^{(21)}e_Le_R^*r_1^{(+)}+2\left[e_L^2+(e_R^*)^2\right]r_3^{(+)}\\&\quad+2\left[e_R^2+(e_L^*)^2\right]r_3^{(-)}-\frac{r_2^{(0)}}{\tau_2},\end{aligned} \tag{A37}$$

$$\partial_\tau r_2^{(+)}=-4\gamma_-^{(12)}e_Re_L^*r_1^{(0)}+2\left[e_R^2+(e_L^*)^2\right]r_3^{(0)}-4(\gamma_-^{(1)}|e_R|^2+\gamma_-^{(2)}|e_L|^2)r_1^{(+)}+8\mathrm{Re}(e_Re_L)r_3^{(+)}-\frac{r_2^{(+)}}{\tau_2}, \tag{A38}$$

$$\begin{aligned}\partial_\tau r_3^{(0)}&=-8\left[\mathrm{Re}(e_Re_L)r_2^{(0)}+\mathrm{Im}(e_Re_L)r_1^{(0)}\right]+2i\left[e_R^2-(e_L^*)^2\right]r_1^{(-)}+2i\left[e_L^2-(e_R^*)^2\right]r_1^{(+)}-2\left[e_L^2+(e_R^*)^2\right]r_2^{(+)}\\&\quad-2\left[e_R^2+(e_L^*)^2\right]r_2^{(-)}-\frac{r_3^{(0)}+1}{\tau_1},\end{aligned} \tag{A39}$$

$$\partial_\tau r_3^{(+)}=2ir_1^{(0)}\left[e_R^2-(e_L^*)^2\right]-2r_2^{(0)}\left[e_R^2+(e_L^*)^2\right]-8[\mathrm{Re}(e_Re_L)r_2^{(+)}+\mathrm{Im}(e_Re_L)r_1^{(+)}]-\frac{r_3^{(+)}}{\tau_1}, \tag{A40}$$

$$(\partial_\tau+\partial_\xi)e_R=\frac{ia_1}{2}\left(\gamma_+^{(1)}+\gamma_-^{(1)}r_3^{(0)}\right)e_R+\frac{i}{2}\gamma_-^{(12)}r_3^{(+)}e_L+\frac{ia_{12}}{2}\left(r_1^{(0)}-ir_2^{(0)}\right)e_L^*+\frac{i}{2}(r_1^{(+)}-ir_2^{(+)})e_R^*, \tag{A41}$$

$$(\partial_\tau-\partial_\xi)e_L=\frac{ia_2}{2}\left(\gamma_+^{(2)}+\gamma_-^{(2)}r_3^{(0)}\right)e_L+\frac{i}{2}\gamma_-^{(21)}r_3^{(-)}e_R+\frac{ia_{21}}{2}\left(r_1^{(0)}-ir_2^{(0)}\right)e_R^*+\frac{i}{2}\left(r_1^{(-)}-ir_2^{(-)}\right)e_L^*. \tag{A42}$$

$$\gamma_\pm^{(a)}=\frac{\mu_{ee}(\omega_a,\omega_a)\pm\mu_{gg}(\omega_a,\omega_a)}{2\mu_{ge}},\qquad \gamma_\pm^{(ab)}=\frac{\mu_{ee}(\omega_a,\omega_b)\pm\mu_{gg}(\omega_a,\omega_b)}{2\mu_{ge}}, \tag{A43}$$

$$a_i=\frac{2\omega_i}{\epsilon_{eg}},\qquad a_{ij}=\frac{2\omega_j^2}{\omega_i\epsilon_{eg}}, \tag{A44}$$

with μ_{ab} defined by Eq. (A15). The single-mode equations in the text are readily derived by taking $\omega_i=\epsilon_{eg}/2, a_i=1, a_{ij}=1$, and all $\gamma_\pm^{(ab)}$ a,b independent.

8. Pulse compression factor

We shall estimate pulse propagation effects neglected in the text. Pulse propagation may be described by ignoring RL mixing terms in the general master equations. By taking one mode e_R of one color, the basic propagation equations are

$$\partial_\tau r_1=4r_3\mathrm{Im}e_R^2+4\gamma_-r_2|e_R|^2-\frac{r_1}{\tau_2}, \tag{A45}$$

$$\partial_\tau r_2=4r_3\mathrm{Re}e_R^2-4\gamma_-r_1|e_R|^2-\frac{r_2}{\tau_2}, \tag{A46}$$

$$\partial_\tau r_3=-4\left(r_1\mathrm{Im}e_R^2+r_2\mathrm{Re}e_R^2\right)-\frac{r_3+1}{\tau_1}, \tag{A47}$$

$$(\partial_\tau+\partial_\xi)e_R=\frac{i}{2}[(\gamma_++\gamma_-r_3)e_R+(r_1-ir_2)e_R^*]. \tag{A48}$$

We shall ignore relaxation terms, taking $\tau_i\to\infty$. The results of Ref. [14] in terms of the area function follow from the assumption of the reality of the function e_R. The relation $r_1=-\gamma_-r_3$ automatically follows from the consistency of three Bloch equations. The fundamental equation of the propagation problem is given by a single nonlinear field equation in terms of the area function $\theta(\xi,\tau)$:

$$e_R^2=\frac{\partial_\tau\theta}{4\sqrt{1+\gamma_-^2}},\quad r_3=\pm\frac{\cos\theta}{\sqrt{1+\gamma_-^2}},\quad r_2=\pm\sin\theta, \tag{A49}$$

$$(\partial_\tau+\partial_\xi)\partial_\tau\theta=\pm\sin\theta\,\partial_\tau\theta. \tag{A50}$$

Analytic solutions of this nonlinear equation give [14] the following.

(1) *Pulse splitting*. The number N of split pulses is given by the pulse area of the initial flux $F_i(t)$ divided by 2π:

$$N=\frac{1}{2\pi}\sqrt{\mu_{ge}^2+(\mu_{ee}-\mu_{gg})^2/4}\int_{-\infty}^{\infty}dyF_i(y). \tag{A51}$$

(2) *Pulse compression*. The pulse of an area $<2\pi$ is compressed by an amount E (result obtained for Lorentzian pulse),

$$E = \frac{1}{[\alpha_m x \sin(\tilde{\theta}/2) \pm \cos(\tilde{\theta}/2)]^2 + \sin^2(\tilde{\theta}/2)}, \quad \text{(A52)}$$

$$\tilde{\theta} = \sqrt{\mu_{ge}^2 + (\mu_{ee} - \mu_{gg})^2/4} \int_{-\infty}^{t-x} dy F_i(y), \quad \text{(A53)}$$

$+(-)$ corresponding to amplifier(absorber).

We may estimate the pulse compression factor (A52) for cw trigger irradiation of duration t in which case $\tilde{\theta} \sim \beta t$:

$$E = \frac{1}{(\beta t \alpha_m x \pm 1)^2 + (\beta t)^2} \sim \frac{1}{1 \pm 2\beta t \alpha_m x}. \quad \text{(A54)}$$

In all cases of interest $\beta t \leqslant \beta T_2 \ll 1$. Thus, unless the target length is large enough, close to $1/(2\beta T_2 \alpha_m)$, the effect of pulse compression is not large.

APPENDIX B: EXACT AND APPROXIMATE CONSERVATION LAWS

We focus on the degenerate case of $\omega_1 = \omega_2 = \epsilon_{eg}/2$. There are three different classes of exact and approximate conservation laws: (1) one exact conservation that holds with finite T_i, (2) another approximate conservation law that holds in the $T_1 \to \infty$ limit, (3) one last approximate conservation law that holds in the $T_2 \to \infty$ limit ($T_1 \gg T_2$ assumed).

The first exact conservation law is derived directly from two equations of motion for the field e_i, and it reads as

$$(\partial_\tau + \partial_\xi)|e_R|^2 = (\partial_\tau - \partial_\xi)|e_L|^2. \quad \text{(B1)}$$

An integral form of this conservation for a finite target of length L ($l = \alpha_m L$ below) is

$$\frac{d}{d\tau} \int_0^l d\xi (|e_R|^2 - |e_L|^2) = -[|e_R|^2 + |e_L|^2]_{\xi=0}^l. \quad \text{(B2)}$$

The integrated quantity of $|e_R|^2 - |e_L|^2$ stored in the target balances against its flux outgoing from two target ends. For the symmetric trigger, the right-hand side of this equation vanishes, and the integral on the left-hand side is a constant of motion.

The second conservation law that holds in the $T_1 \to \infty$ limit is

$$\partial_\tau [r_3 + 4(|e_R|^2 + |e_L|^2)] + 4\partial_\xi (|e_R|^2 - |e_L|^2) = 0, \quad \text{(B3)}$$

corresponding to the energy conservation. The energy density inside the target is the sum of the medium and field energies, $r_3/2 + 2(|e_R|^2 + |e_L|^2)$, in our dimensionless unit. The integrated form of this conservation law in the real unit is

$$\frac{d}{dt} \int_0^L dx \left(\frac{\epsilon_{eg}}{2} R_3 + 2(|E_R|^2 + |E_L|^2) \right) = -2[|E_R|^2 - |E_L|^2]_{x=0}^L. \quad \text{(B4)}$$

The third class of conservation law that holds in the $T_2 \to \infty$ limit is

$$\partial_\tau (r_1^2 + r_2^2 + r_3^2) = 0. \quad \text{(B5)}$$

APPENDIX C: HELICAL SOLITON

A new type of topological soliton may exist because the basic equation has two components $\varphi^{(i)}(\xi), i = 1,2$, and one can give a topological quantum number in $1+1$ dimensions, as illustrated in Fig. 15. For simplicity assume a field with two real components (X,Y) and its periodicity with a period of the target length $l(= \alpha_m L)$ or a few times this length. We may define the homotopy class [27] of the mapping of a circle $x + iy = le^{i\xi}, 0 \leqslant \xi \leqslant 2\pi$ in two-dimensional real space onto the field space of the unit magnitude, $X^2 + Y^2 = 1$. The winding number w is defined using the complex field $Z = X + iY = e^{i\varphi(\xi)}$:

$$w = -i \int_0^{2\pi} \frac{d\xi}{2\pi} Z^* \partial_\xi Z = \frac{\varphi(2\pi) - \varphi(0)}{2\pi}. \quad \text{(C1)}$$

When this winding number is quantized, $w = n, n = 0, \pm 1, \pm 2, \ldots$, the winding number is topologically stable and conserved during time evolution.

The correspondence to static solutions in Sec. V is as follows. One considers the real three-vector field $\vec{X}(\xi)$ of unit length, $(X,Y,Z) = (\cos\varphi, \cos S \sin\varphi, \sin S \sin\varphi)$ with φ and S identified as the phase variables in static solutions, and a mapping of the unit circle $0 \leqslant \xi \leqslant 2\pi$ onto $\vec{X}(\xi)$ space. Two solutions of Eqs. (31) and (32) corresponding to two different fundamental regions, $[0,\pi/2]$ and $[\pi/2,\pi]$, are connected together at $\xi = \pi/2$. Then, in the return trip of $\xi = \pi/2 \to \pi$ from the right edge to the left edge of the soliton, the orientation of $\vec{X}(\xi)$ is further advanced forward (dictated by the continuity of solutions) and finally comes back with $\vec{X}(\pi) = -\vec{X}(0)$ at the left edge. This means that solutions of $\vec{X}$ are two-valued representations, namely, spinors.

[1] P. P. Sorokin and N. Braslau, IBM J. Phys. Rev. **8**, 177 (1964); R. L. Garwin, *ibid.* **8**, 338 (1964); A. M. Prokhorov, Science **149**, 828 (1965).

[2] E. M. Belenov and I. A. Poluektov, Zh. Eksp. Teor. Fiz. **56**, 1407 (1969) [Sov. Phys. JETP **29**, 754 (1969)].

[3] L. M. Narducci, W. W. Eidson, P. Furcinitti, and D. C. Eteson, Phys. Rev. A **16**, 1665 (1977).

[4] S. E. Harris, J. E. Field, and A. Imamoglu, Phys. Rev. Lett. **64**, 1107 (1990).

[5] R. L. Shoemaker and R. G. Brewer, Phys. Rev. Lett. **28**, 1430 (1972).

[6] N. Tan-no, K. Yokoto, and H. Inaba, Phys. Rev. Lett. **29**, 1211 (1972).

[7] M. Brune, J. M. Raimond, P. Goy, L. Davidovich, and S. Haroche, Phys. Rev. Lett. **59**, 1899 (1987).

[8] For a review of the experimental and theoretical aspects of EIT, see M. Fleischhauer, A. Imamoglu, and J. P. Marangos, Rev. Mod. Phys. **77**, 633 (2005).

[9] D. J. Gauthier, Q. Wu, S. E. Morin, and T. W. Mossberg, Phys. Rev. Lett. **68**, 464 (1992).

[10] M. Yoshimura, C. Ohae, A. Fukumi, K. Nakajima, I. Nakano, H. Nanjo, and N. Sasao, arXiv:0805.1970; M. Yoshimura, in *Proceedings of 4th NO-VE International Workshop*, edited by M. Baldo Ceolin (Papergraf, Venezia, 2008), p. 311.

[11] For a review of both the theory and experiments of superradiance, see M. Benedict, A. M. Ermolaev, V. A. Malyshev, I. V. Sokolov, and E. D. Trifonov, *Super-radiance: Multiatomic Coherent Emission* (Taylor and Francis, New York, 1996); for a formal aspect of the theory, see M. Gross and S. Haroche, Phys. Rep. **93**, 301 (1982). The original suggestion of superradiance is from R. H. Dicke, Phys. Rev. **93**, 99 (1954).

[12] F. Haake, H. King, G. Schröder, J. Haus, and R. Glauber, Phys. Rev. A **20**, 2047 (1979); D. Polder, M. F. H. Schuurmans, and Q. H. F. Vrehen, *ibid.* **19**, 1192 (1979).

[13] Q. H. F. Vrehen and M. F. H. Schuurmans, Phys. Rev. Lett. **42**, 224 (1979); N. W. Carlson, D. J. Jackson, A. L. Schawlow, M. Gross, and S. Haroche, Opt. Commun. **32**, 350 (1980).

[14] M. Yoshimura, Prog. Theor. Phys. **125**, 149 (2011).

[15] M. Yoshimura, Phys. Lett. B **699**, 123 (2011); Phys. Rev. D **75**, 113007 (2007).

[16] S. L. McCall and E. L. Hahn, Phys. Rev. **183**, 457 (1969). For a review, see L. Allen and J. H. Eberly, *Optical Resonance and Two-Level Atoms* (Dover, New York, 1975). For comparison with experimental results, see R. E. Slusher and H. M. Gibbs, Phys. Rev. A **5**, 1634 (1972).

[17] D. D. Yavuz, Phys. Rev. A **75**, 041802(R) (2007), and references therein.

[18] W. Kolos and L. Wolniewicz, J. Chem. Phys. **46**, 1426 (1967).

[19] The parameter μ_{ab} may also be estimated from $E1$ coupling data of an electronically excited $B \to X$ transition including Franck-Condon vibrational overlap factors, given by the calculation of U. Frantz and D. Wünderlich, International Atomic Energy Agency, Report No. INDC(NDS)-457, 2004 (unpublished). This estimate gives consistent results with the polarizability of [18].

[20] G. Lindblad, Commun. Math. Phys. **48**, 119 (1976).

[21] J. J. Sakurai, *Advanced Quantum Mechanics* (Addison-Wesley, Reading, MA, 1967).

[22] The field equation, Eqs. (9) and (10) and (A29) and (A30), may also be derived by computing the macroscopic polarization vector, as done in Refs. [3,14] for the more restricted case.

[23] M. Lewenstein and K. Rażewski, Phys. Rev. A **26**, 1510 (1982).

[24] E. R. Golubyatnikova, V. V. Kocharovskii, and Vl. V. Kocharovskii, Quantum Electron. **24**, 791 (1994).

[25] For a review of STIRAP, see K. Bergmann, H. Theuer, and B. W. Shore, Rev. Mod. Phys. **70**, 1003 (1998).

[26] A. A. Kalinkin, A. A. Kalachev, and V. V. Samartsev, Laser Phys. **14**, 71 (2004), and references therein.

[27] S. Coleman, *Aspects of Symmetry* (Cambridge University Press, Cambridge, 1985).